

Precession driven low-latitude hydrological cycle paced by shifting perihelion

Hu Yang¹, Xiaoxu Shi¹, Xulong Wang², Qingsong Liu³, Yi Zhong³, Xiaodong Liu², Youbin Sun², Yanjun Cai⁴, Fei Liu⁵, Gerrit Lohmann⁶, Martin Werner⁶, Zhimin Jian⁷, Tainã M. L. Pinho⁶, Hai Cheng⁴, Lijuan Lu^{5,1}, Jiping Liu^{5,1}, Chao-Yuan Yang¹, Qinghua Yang^{5,1}, Yongyun Hu⁸, Xing Cheng⁹, Jingyu Zhang³, and Dake Chen¹

¹Southern Marine Science and Engineering Guangdong Laboratory, Zhuhai, China

²State Key Laboratory of Loess and Quaternary Geology, Institute of Earth Environment, Chinese Academy of Sciences, Xi'an, China

³Centre for Marine Magnetism, Department of Ocean Science and Engineering, Southern University of Science and Technology, Shenzhen, China

⁴Institute of Global Environmental Change, Xi'an Jiaotong University, Xi'an, China

⁵School of Atmospheric Sciences, Sun Yat-sen University, Zhuhai, China

⁶Alfred Wegener Institute, Helmholtz Centre for Polar and Marine Research, Bremerhaven, Germany

⁷Laboratory of Marine Geology, Tongji University, Shanghai, China

⁸Department of Atmospheric and Oceanic Sciences, School of Physics, Peking University, Beijing, China

⁹ShanXi Experimental Center of Geological Survey, ShanXi Institute of Geological Survey, Xi'an, China

Correspondence: Hu Yang (yanghu@sml-zhuhai.cn)

Abstract. Paleoclimate proxies reveal a significant precessional impact on the low-latitude hydrological cycle. Classical theory suggests that precession modulates the inter-hemisphere summer insolation difference, and hence controls the meridional displacement of the Inter-Tropical Convergence Zone. Accordingly, low-latitude precipitation variations are expected to be in-phase (for the Northern Hemisphere) or anti-phase (for the Southern Hemisphere) with the Northern Hemisphere summer insolation. However, increasing number of proxies, particularly those absolutely dated ones, reveal that variations in terrestrial precipitation at different low-latitudes follow distinct precession rhythms that are very often out-of-phase with hemispheric summer insolation. The mechanism underlying such spatial-temporal complexity remains elusive. In this study, we argued that the precession-driven-performed theoretical analysis, climate simulations, and geological records to hypothesize that the low-latitude hydrological cycle is paced by shifting perihelion, rather than the hemispheric summer insolation. More specifically, precession of the Earth's rotation axis alters the occurrence shifts the season and latitude of perihelion. When perihelion occurs, increasing insolation raises the moist static energy over Here, the latitude of perihelion is introduced as the latitude of Earth's subsolar point during perihelion, which is the location where the most intense solar radiation is concentrated. At the time of perihelion, intense solar radiation heats the land faster than over the ocean due to differing thermal inertia. This thermodynamically moves the tropical convergence precipitation convection from the ocean to the land, contributing to enhancing the terrestrial precipitation over the latitudinal rain belt. As perihelion shifts towards different latitudes and seasons at different precessional phases, this leads asynchronous terrestrial precipitation maxima around the perihelion latitude. As the precessional phase changes, perihelion moves toward different latitudes, causing asynchronous maximums in terrestrial precipitation at dif-

ferent latitudes. ~~Our hypothesis, supported by both model simulations and geologic records, suggests that~~ Perihelion can occur in any season; therefore, the insolation in individual seasons is equally important in shaping the ~~orbital-scale~~ orbital-scale climate changes at ~~low-latitude~~ low latitudes. This offers ~~an alternative dynamical interpretation for the complex evolution of low-latitude hydrological cycle under precessional forcing~~ new insight into the Milankovitch theory, which highlights summer insolation's role in shaping orbital-scale climate change.

1 Introduction

By redistributing solar radiation across different latitudes and seasons, Earth's orbital changes exerted a significant impact on past climate change (Milankovitch, 1941; Berger, 1978, 1988). In high-latitude regions, these orbital-scale climate changes are ~~eharacterised~~ characterized by cyclic expansion and retreat of ice sheets, with periodicities of ~ 41 or ~ 100 kilo-years (ka) (Lisiecki and Raymo, 2005), modulated by the Milankovitch cycles of obliquity and eccentricity (Milankovitch, 1941). In contrast, low-latitude climate changes are marked by periodic variations in hydrological cycle with dominant period of ~ 23 ka, aligning with the Milankovitch cycles of precession (Clement et al., 2004; Cruz Jr et al., 2005; Braconnot et al., 2008; Carolin et al., 2013; Cheng et al., 2016; Wang et al., 2014a; Cheng et al., 2022). These precessional fluctuations are widely documented in the precipitation-related proxies from ~~Asia, South America, and Africa~~ (Kutzbach, 1981; Kuper and Kropelin, 2006; An et al., 2000; Cruz Jr et al., 2005; Kuper and Kropelin, 2006; Hély et al., 2014; El-Shenawy et al., 2018), Asia (An et al., 2000; Wang et al., 2007, 2014a), Australia (Beaufort et al., 2010) and South America (Baker et al., 2001; Wang et al., 2004; Cruz Jr et al., 2005). Among these changes, the periodic greening of the Sahara stands out as one of the most fascinating phenomena ~~(Kutzbach, 1981; Kuper and Kropelin, 2006; DeMenocal et al., 2012; Armstrong et al., 2023).~~

~~Low-latitudes~~ Low-latitude precipitation primarily comes from the seasonal north-south migration of the Inter-Tropical Convergence Zone (ITCZ, ~~Fig. 1a~~), which follows the march of the Earth's thermal equator (Fig. 1) (Gadgil, 2018). Early studies proposed that precession regulates the inter-hemispheric summer insolation difference and modulates the meridional migration of the ITCZ (Kutzbach, 1981; Wang et al., 2014a; Schneider et al., 2014). Increased ~~summer insolation in the Northern Hemisphere~~ Northern Hemisphere summer insolation (perihelion) corresponds to decreased ~~summer insolation in the Southern Hemisphere~~ Southern Hemisphere summer insolation (aphelion). Accordingly, variations in ~~terrestrial~~ ITCZ precipitation are expected to align with changes in summer insolation, exhibiting an anti-phase relationship between the Northern and Southern Hemispheres ~~(Wang et al., 2004; Cruz Jr et al., 2005; Cheng et al., 2013; Wang et al., 2014a, 2017)~~ (Wang et al., 2004; Cruz Jr et al., 2005; Cheng et al., 2013; Wang et al., 2014a, 2017) (Fig. ~~1b and 1d~~ 2b and 2d). However, in the past two decades, an increasing number of proxies have shown that although low-latitude terrestrial precipitation displays significant precessional variations, their evolution patterns are not necessarily in-phase with the Northern/Southern Hemisphere summer insolation ~~(An et al., 2000; Clemens and Prell, 2007; Carolin et al., 2013, 2016; Zhou et al., 2022)~~ (An et al., 2000; Wang et al., 2004; Clemens and Prell, 2007; Carolin et al., 2013, 2016; Zhou et al., 2022). For example, the reconstructed ~~onsets and~~ optimums of the East Asian summer monsoon at different geographical locations were asynchronous with ~~the Northern Hemisphere summer insolation~~ each other, suggesting that the precipitation optimum doesn't occur all at the same time (An et al., 2000; Cai et al., 2010; Ran and Feng, 2013; Chen et al., 2015; Liu et al., 2015; Zhou et al., 2022). The

Indian summer monsoon, reconstructed from sediment cores of the Arabian Sea, shows an early Holocene optimum (Thamban et al., 2007), significantly preceding that of the East Asian summer monsoon (Sun et al., 2006; Liu et al., 2015). ~~Around the Over Africa, archaeological and geological evidence indicates that the recent termination of the greening Sahara shows time-transgressive pattern, occurred earlier in north Africa than in the south (Kuper and Kropelin, 2006; Shanahan et al., 2015)~~
55 ~~. Speleothem records and travertine deposits collected around northeastern Brazil (10°S) suggested that the local wet periods presented themselves during the high insolation periods of austral autumn rather than austral summer (Wang et al., 2004). Near the equator, a Malaysian speleothem $\delta^{18}O$ record, reflecting local precipitation strength, exhibits an evolutionary pattern neither comparable to the Northern Hemisphere summer insolation nor the Southern Hemisphere summer insolation, but insolation in October (Carolin et al., 2013) (Fig. 1e).~~ ~~Over Africa, archaeological and geological evidence indicates that the recent~~
60 ~~termination of the greening Sahara occurred earlier in north Africa than in the south (Kuper and Kropelin, 2006; Shanahan et al., 2015) -2c).~~

The cause of the asynchronous relationship between terrestrial precipitation and summer insolation has been investigated extensively from both modelling and proxy-model comparison perspectives (Short and Mengel, 1986; Braconnot and Marti, 2003; Zhao et al., 2005; Kuper and Kropelin, 2006; Clemens and Prell, 2007; Shanahan et al., 2015; Ran and Feng, 2013; Chen
65 et al., 2015; Cheng et al., 2021; Zhou et al., 2022). These studies ~~hypothesis-propose~~ that summer insolation's control on the ~~low-latitude~~ hydrological cycle could be disrupted by a variety of factors, including fluctuation of CO₂ (Lu et al., 2013; McGrath et al., 2021),
internal ocean-atmosphere feedback (Clemens and Prell, 2007), present (Clemens and Prell, 2007; Carolin et al., 2013, 2016),
presence of ice sheet (Chen et al., 2015), development of vegetation (Cheng et al., 2021), (Chiang and Bitz, 2005; Chen et al., 2015; Wu et al., 2015),
delayed ocean warming (Ran and Feng, 2013) and sea level fluctuations (Griffiths et al., 2009) (Griffiths et al., 2009; Windler et al., 2021)
70 and millennial-scale abrupt climate changes originating from high latitudes (Wang et al., 2008; Chiang and Friedman, 2012).
Interestingly, transient and time-slice simulations with solely insolation forcing also yield an asynchronous precipitation response to hemispheric summer insolation ~~(Braconnot and Marti, 2003; Kutzbach et al., 2008; Erb et al., 2015; Liu et al., 2022)~~
~~(Braconnot and Marti, 2003; Kutzbach et al., 2008; Erb et al., 2015; Bischoff et al., 2017; Liu et al., 2022)~~. This raises question
of whether terrestrial precipitation ~~does not follow~~ follows (or not) changes in hemispheric summer insolation. By performing
75 simulations with different precessional phases, Braconnot and Marti (2003) found that the ~~occurrence-time~~ calendar timing
of maximum insolation (perihelion) ~~affect~~ affects the seasonality of Indian monsoon. They proposed that insolation in other
seasons may also important, especially in determining the seasonal timing of Indian summer monsoon. Focusing on the East
Asian monsoon, Zhou et al. (2022) suggested that insolation in different months may contribute to a time-transgressive pattern of East Asian monsoon ~~optimum at different latitudes~~ optimums, with earlier occurrence in the southern China and later
80 occurrence in the northern area. By running an isotope-enabled transient simulation covering the past 300 ka, Liu et al. (2022)
found that the precipitation $\delta^{18}O$ in Asia is primarily affected by the temperature and insolation during the rainy seasons, rather
than the averaged boreal summer insolation.

In this study, we ~~performed present~~ theoretical analysis, climate ~~simulations and geological records, to hypothesis that model~~
simulations, and synthesis of geologic records from different latitudes to hypothesize that the precession-driven low-latitude
85 hydrological cycle is ~~paced-regulated~~ by shifting perihelion ~~, rather than the hemispheric summer insolation across different~~

seasons and latitudes. Consequently, the precipitation optimums at different latitudes occurs in a naturally asynchronous manner.

2 Methodology

2.1 Model Simulations

90 Using ~~AWI~~Alfred Wegener Institute Earth System Model (AWI-ESM, (Sidorenko et al., 2015, 2019)), we ~~perform~~conduct two set of experiments to study the ~~mechanism of precessional impact on dynamics of precession-driven~~ low-latitude hydrological cycle. The AWI-ESM is a coupled ocean-atmosphere model. ~~It consists of,~~ consisting the atmospheric component ECHAM6 (Giorgetta et al., 2013) and the oceanic component FESOM (Wang et al., 2014b; Danilov et al., 2017). The oceanic component employs an unstructured-mesh, with relatively high resolution (up to 25 km) at polar regions, coast areas and the equator, while the atmospheric component has a spatial resolution of 1.875°. ~~Detailed~~In our experiments, we implement a dynamic vegetation, which dynamically alters the vegetation coverage and the surface albedo in response to climate changes. More detailed information on the model setup can also be found in ~~Shi et al. (2016) (Shi and Lohmann, 2016)~~Shi and Lohmann (2016).

2.1.1 Idealised Earth system without tilted Earth rotation axis

100 In the first experiment, we create an idealised Earth system without seasonal migration of ~~Sun's zenith~~Earth's subsolar point (obliquity=0), while introducing a relatively elliptical Earth's orbit (eccentricity=0.058). In this experiment, perihelion takes place in June and aphelion takes place in December. We run the simulation for 1000 years, with the last 100 years result used for analysis. This experiment is designed ~~aiming to test how changing to examine how changing the~~ Earth-Sun distance affects the, or perihelion, affects tropical precipitation over land.

105 2.1.2 Simulations reconstructing a precessional cycle

In the second ~~step~~experiment, we perform ~~another set of experiments~~a set of simulations to reconstruct the climate change within a precessional cycle. In these simulations, the obliquity is set to be 24.5°. Twenty-four sensitivity simulations were ~~performed~~ran using different precessional phases, i.e., 0°, 15°, 30°, ... 345°. To allow the low-latitude climate to reach a quasi-equilibrium state to insolation forcing, we integrated the model for 300 years, and the last 100 years mean climate were
110 used to represent the climate at the corresponding precession phase. ~~This approach removes the natural climate variability, such as El Nino-Southern Oscillation.~~

All these 24 simulations are initialized from a pre-industrial simulation which had participated in the PMIP4 project (Kageyama et al., 2018). For all simulations, the greenhouse gas concentrations in the atmosphere, land-sea distribution and ice sheet configuration are fixed as the pre-industrial condition.

115 Natural climate variability is ubiquitous that sometimes conceals external forcing. To highlight the external precessional forcing in climate change, in all simulations, the eccentricity is set to a relatively high value (0.058), which represents the highest eccentricity during the quaternary (Berger, 1978). Consequently, this configuration exposes the Earth to 26% more solar radiation during perihelion than during aphelion. Additionally, we examine the climatology mean of the last 100 years model results. This further eliminates the ~~contribution of natural variability on simulated climate changes~~ climate noise from natural variability.

~~Due to differences~~ The definition of seasonality, which is influenced by slow variations in the Earth's ~~revolution speed~~, 's orbit, plays a key role in determining the calculated seasonal cycle of the ~~length of four seasons varies depending on the precessional configurations. This leads the "calendar effect"~~ climate. Application of the Gregorian calendar where the lengths of the months and seasons are fixed results in a drift in the occurrence date of different seasons. Especially, the applied high eccentricity (0.058) leads to a shift in the date of the autumn equinox by up to 27 days within our simulations. This may lead artificial biases when comparing monthly temperature and precipitation across different simulations with different precessional phases (Kutzbach and Gallimore, 1988; Joussaume and Braconnot, 1997). In contrast to the "~~(Joussaume and Braconnot, 1997; Shi et al., 2022)~~ ~~In our results, we use the present day calendar, with the spring equinox set at March 21. As a results, the dates of the summer solstice, autumnal equinox, and winter solstice can be changed a couple of days depending on the precessional configurations. Since our analysis is based on monthly results, we do not make any additional corrections on these dates in order to keep consistency.~~ fix-day" Gregorian calendar widely used today, the angular calendar calculates the lengths of the months and seasons according to a fixed angle along the Earth's orbit. When comparing simulation results for different orbital configurations, it is essential to use the angular calendar to ensure that the data for comparison are from the same position along the Earth's orbit (Joussaume and Braconnot, 1997; Pollard and Reusch, 2002). To address this, we applied a calendar correction on our model results (temperature, precipitation, insolation) by changing the monthly mean data from the Gregorian calendar to an angular calendar. Detailed methodology can be found in Shi et al. (2022).

2.2 Speleothem ~~Proxies~~proxies

~~Speleothem~~ With precise chronologies and widespread distribution, speleothem records are widely used to reconstruct the past hydrological cycle (Kaushal et al., 2024). To verify our hypothesis, we synthesize the speleothem $\delta^{18}O$ records from China (~~Cheng et al., 2016~~), Malaysia (~~Carolin et al., 2013, 2016~~) and Brazil (~~Cruz Jr et al., 2005~~) are used in this study. Malaysia and Brazil. The record from China is composited by (~~Cheng et al., 2016~~) Cheng et al. (2016) based on several ~~records~~ samples from Sanbao (31° 40' N, 110° 26' E), Hulu (32° 30' N, 119° 10' E), and Dongge (25° 17' N, 108° 5' E) caves (Wang et al., 2001; Dykoski et al., 2005; Kelly et al., 2006; Wang et al., 2008; Cheng et al., 2009). The Malaysia records were collected in different caves in Gunung Mulu National Park, Borneo, Malaysia (~~4°~~ 4°N, 115°E) (Carolin et al., 2013, 2016). The Brazil record is collected from the Botuvera Cave (27° 13' 24" S, 49° 09' 20" W) (Cruz Jr et al., 2005). These $\delta^{18}O$ records are believed to represent the changes in local precipitation amounts, as indicated by the original publications (Cruz Jr et al., 2005; Carolin et al., 2013; Che

2.3 Method

The Empirical orthogonal functions (EOF) analysis is used to identify the spatial and temporal characteristics of terrestrial precipitation at low latitudes. EOF analysis is widely applied in Earth science. It is generally used to simplify a spatial-temporal data set by converting it into spatial patterns of variability and temporal evolution of these patterns. For the idealised Earth system experiment without tilted Earth rotation axis, we applied EOF analysis on the climatology monthly convective precipitation (Fig. 3). For the 24 simulations recovering

2.3.1 Calculation of solar radiation pattern

To understand how the solar radiation fluctuates throughout a precessional cycle, we ~~applied EOF analysis on the individual monthly convective precipitation. For example, December precipitation in the 24 simulations are selected and applied a EOF analysis to generate Fig. 4~~ compute seasonal solar radiation patterns using MATLAB with aids from two tools, namely, "Orbital, the Box" (Lougheed, 2021) and the Earth Orbit Model v2.1 (Kostadinov and Gilb, 2014). These tools were developed based on the theoretical framework presented in (Berger, 1978; Laskar, 1990; Laskar et al., 1993).

2.3.2 Tracking the thermal equator

The ITCZ precipitation takes place over the Earth's warmest region, i.e., the thermal equator. To ~~determine the geographical location of the thermal equator, we calculate the~~ understand the movement of tropical precipitation, we track the thermal equator based on moist static energy (analogous to equivalent potential temperature) using the following equation:

$$S = C_p \cdot T + g \cdot z + L_v \cdot q \quad (1)$$

where S is the moist static energy, C_p is the specific heat at constant pressure, T is the absolute air temperature, g is the gravitational constant, z is the geopotential height above sea level, L_v is the latent heat of vaporization, and q is water vapor specific humidity (Neelin and Held, 1987; Wallace and Hobbs, 2006).

~~The latitude of the perihelion is introduced as the latitude of Sun's zenith point when perihelion occurs. This latitude also represents the latitude of maximum incoming solar radiation at the top of atmosphere. The insolation characteristics are calculated using MATLAB with aids from two tools, namely the "Orbital, The region with the highest moist static energy is the Box" (Lougheed, 2021) and the Earth Orbit Model v2.1 (Kostadinov and Gilb, 2014). These tools were developed based on the theoretical framework presented in (Berger, 1978; Laskar, 1990; Laskar et al., 1993).~~ thermal equator, where deep convection occurs (Barry and Chorley, 2009).

2.3.3 Empirical orthogonal functions analysis

The Empirical Orthogonal Functions (EOF) analysis (Hannachi et al., 2007) is used to identify the spatial and temporal characteristics of terrestrial precipitation at low latitudes. EOF analysis is widely applied in Earth science. It is generally used to simplify a

spatial-temporal data set by converting it into spatial patterns of variability and temporal evolution of these patterns. For the idealised Earth system experiment without tilted Earth rotation axis, we applied EOF analysis on the climatology monthly convective precipitation (Fig. 4). For the 24 simulations recovering a precessional cycle, we applied EOF analysis on the individual monthly convective precipitation. For example, December precipitation in the 24 simulations is selected and applied a EOF analysis to generate Fig. 5a.

3 Precession shifts the season and latitude of perihelion

To understand the mechanism of how precession governs the low-latitude hydrological cycle, we first look at how precession affects the solar radiation received by the Earth.

The Earth's orbit around the Sun is not a perfect circle, but an ellipse. When the Earth's distance from the Sun is at its shortest, i.e., perihelion, it receives the strongest solar radiation. Currently, perihelion happens in boreal winter, when the SunEarth's zenith-subsolar point closes to the Tropic of Capricorn (Fig. S2d). By changing the orientation of the Earth's rotation axis, precession gradually delays the occurrence-calendar timing of perihelion by around 20.4-25.1 minutes per year. This is equivalent to the Earth's subsolar point at perihelion migrating by about 500 meters per year. About 11 kiloyears ago, perihelion occurred in boreal summer, when the SunEarth's zenith-point-subsolar point was closest to the Tropic of Cancer (Hunt et al., 2023) (Fig. S2b). Therefore, precession not only shifts the occurrence-season-of-perihelion, calendar timing of perihelion but also the "latitude of perihelion". Here, we introduce the latitude of perihelionis introduced as, which is the latitude of Sun's zenith point when perihelion occurs. Supplementary Movie 1 further clarify this. Earth's subsolar point during perihelion (Fig. S2). This latitudinal zone represents the region with the most intense incoming solar radiation. Logically, it also corresponds to the strongest thermal equator if the solar heating effect is instantaneous.

To precisely-describe-detail when and where perihelion occurs, Fig. 2-details-the-season-3 shows the calendar timing and latitude of perihelion at different precessional phases (longitude of perihelion). Similar to the movement of the Sun's-zenith Earth's subsolar point over the course of a year, the latitude of perihelion migrates between the Tropics of Cancer and Capricorn over the course of a precessional cycle. Supplementary Movie 1 further clarifies this. Whenever (the season) and wherever (the latitude) perihelion occurs, the insolation-solar radiation in the corresponding season and the perihelion latitude reaches its maximum in a precessional cycle(Supplementary Movie 1). Maximum insolation-(perihelion)-potentially-drives-anomalous climate-changes-on-Earth.

4 Perihelion promotes tropical convective precipitation over land

To investigate how perihelion impacts low-latitude climate change, we conducted an idealised Earth system experiment using AWI-ESM(Sidorenko et al., 2015, 2019). In this idealised Earth system, the Earth's rotation axis is not tilted (zero obliquity). The Earth's orbit is set to be relatively elliptical (see Model SimulationsSection 2.1.1). As a result, the thermal equator and the

associated tropical rain belt are constrained in the vicinity of the geographic equator. However, due to variations in the distance between ~~Earth and Sun, the~~ the Earth and the Sun, temperature and precipitation ~~exhibits~~ exhibit a seasonality (Fig. 34).

~~When perihelion occurs~~ At perihelion, the incoming solar radiation maximises. Due to the different thermal inertia between
210 the land and the ocean, the atmospheric heating over land is ~~much~~ stronger than that over the ocean. This leads to a faster increase in moist static energy over ~~the land than~~ land than over the ocean (Fig. S2S3). As tropical ~~convective precipitation~~ deep convection tends to occur towards the warmest regions with the highest moist static energy (Neelin and Held, 1987; Battisti et al., 2014; Schneider et al., 2014; Geen et al., 2020), we observed maximum convective precipitation over land ~~(minimum convective precipitation over ocean)~~ 1-2 month months after the perihelion (Fig. 3 and S24). In brief, perihelion ~~can~~ promote ~~promotes~~ tropical precipitation over land. With this understanding, we switch to a more complex Earth system with a
215 tilted Earth's rotation axis and shifting perihelion.

5 Seasonal terrestrial precipitation peaks whenever and wherever perihelion occurs

~~We~~ The above experiment depicts a very idealized Earth. To simulate the climate in a more realistic world, we conducted another set of numerical experiment using AWI-ESM. This time, the Earth's rotation axis is tilted (obliquity=24.5°). Therefore,
220 the ~~Sun's zenith~~ Earth's subsolar point marches between the Tropics of Cancer and Capricorn, driving a seasonal migration of ITCZ and terrestrial precipitation (Fig. S31). We manipulated precessional phase to reconstruct the climate changes over the course of a precessional cycle (see Methodology Section 2.1.2). Specifically, 24 time-slice simulations were performed with the precessional phase (namely the longitude of the perihelion) varying from 0° to 345° with an interval of 15° (Fig. 2). Due to different precessional phases, when (the ~~season~~ calendar timing) and where (the latitude) the perihelion takes place vary among
225 these experiments (Fig. 23).

~~Since the~~ Because low-latitude ~~terrestrial land~~ precipitation is concentrated at different latitudes in different months ~~, we~~ examined for each individual month the precipitation evolution in a precessional cycle. Empirical Orthogonal Functions (EOF) ~~(Fig. 1), we investigate how precipitation evolves in each month over a precession cycle.~~ EOF analysis was applied to explore the spatial and temporal characteristics of terrestrial precipitation oscillation. This allows us to identify where (the
230 ~~latitudes~~ geographical location) and when (the precessional phase) the terrestrial precipitation peaks.

In February, the ITCZ and predominant terrestrial precipitation locates at its southernmost latitudes (Fig. 4f1 and 5f, contours). ~~We found the strongest February terrestrial precipitation~~ EOF analysis on the February precipitation reveals that the strongest terrestrial precipitation is around precessional phase of -75° (Fig. 4f5f, blue line). This corresponds to the perihelion occurring ~~one~~ 1.5 month earlier (in early January, as shown in Fig. 4f5f with a colored circle) at its southernmost latitudes.

235 The ITCZ and associated rain belt locates around the equator in April (Fig. 4e1 and 5e, contours). We found the strongest April precipitation around the precessional phase of 15° (Fig. 4e5e, blue line) when perihelion occurs in March, with the latitude of perihelion being around the equator (Fig. 4e5e, colored circle).

Following the seasonal migration of ~~Sun's zenith~~ Earth's subsolar point, the rain belt moves northward and reaches its northernmost position in August (Fig. ~~4e1 and 5c~~ 4e1 and 5c, contours). Within a precession cycle, August terrestrial precipitation peaks

240 near precessional phase of 120° (Fig. 4e5c, blue line), corresponding to a late July perihelion. This means that the perihelion latitude is almost at its northernmost ~~latitudes~~ position (Fig. 4e5c, colored circle).

From August to February, the terrestrial precipitation migrates southward, completing an annual cycle ~~-(Fig. 1)~~. Whenever (the season) and wherever (the latitude) perihelion occurs, the related seasonal and latitudinal terrestrial precipitation reaches its maximum. This leads asynchronous terrestrial precipitation ~~maxima~~ optimum at different seasons and latitudes (Fig. 45, blue arrow in the left panels).

There is good co-variation between the seasonal insolation intensity (Fig. 45, black lines), land surface temperature (Fig. 45, red lines) and terrestrial precipitation (Fig. 45, blue lines). We propose that perihelion ~~maximises~~ maximizes the incoming solar radiation and drives the greatest land-sea heating contrast. This thermodynamically moves the ~~tropical convergence zone~~ thermal equator and the corresponding tropical convection from ocean to land (Fig. S4) (Battisti et al., 2014), and forces the strongest seasonal terrestrial precipitation within a precessional cycle. Due to the ~~thermal inertia of the Earth~~ Earth's thermal inertia, the thermal equator and seasonal terrestrial precipitation ~~do not synchronise~~ are not synchronized with the insolation in the same month, but ~~rather the insolation at approximately~~ the insolation about 1-2 ~~month~~ months earlier. In agreement, such a delay has been also revealed by many other model simulations (Kutzbach et al., 2008; Erb et al., 2015; Donohoe et al., 2020; Liu et al., 2022).

255 ~~Moving perihelion introduces strongest solar radiation across~~ In a precessional cycle, the perihelion shifts toward different seasons and ~~latitudes, and forces strongest~~ perihelion latitudes. This results in the strongest solar radiation and terrestrial precipitation in the corresponding season and latitudes (Fig. 56). Theoretically, for the tropical ~~area~~ latitudes between the Tropics of Cancer and Capricorn, there are two ~~occurrences of perihelion~~ passages of perihelion latitude within a precession cycle. For instance, at the equator, the first perihelion passage occurs at precessional phase of 0° around the spring equinox (Fig. 23). The second perihelion passage occurs at precessional phase of 180° around the autumnal equinox (Fig. 23). Consequently, at the equator, the temporal interval between these two perihelion ~~events~~ passages spans half of a precessional cycle, resulting in cyclic variations in precipitation with a period of half of a precession cycle (Fig. 5e6c).

For the area outside the equatorial zone, the time interval between the two successive perihelion ~~events~~ passages varies across different latitudes (Fig. 2-3 and Supplementary Movie 1). With increasing latitude, these two perihelion ~~events~~ passages take place closer to each other, and merge into a single insolation and precipitation maximum at latitudes higher than the Tropic of Cancer (Fig. 23). This phenomenon is evident in our analysis of monthly precipitation patterns derived from zonal mean precipitation in different latitudinal belts (Fig. 56).

6 Evidence from geologic records

Besides model simulations, a realistic precession cycle can also be examined in the sparse-distributed geologic archives. There is a relatively abundant collection of proxies for the most recent precession cycle, spanning the past 23 ka. However, these records may not be ideal for deriving precession-associated climate changes, due to the limitation of the relatively low eccentricity (Berger, 1978, 1988), which diminishes the influence of precession on driving climate variations (Fig. S57) (Braconnot

and Marti, 2003; Bosmans et al., 2018; Chiang et al., 2022; Beaufort and Sarr, 2023; Wu et al., 2023a). Moreover, the scenario becomes more complex due to a variety of factors, such as the rapid disintegration of ice sheets, rising sea level, increasing greenhouse gas concentrations, and abrupt climate changes (Griffiths et al., 2009; Weber and Tuenter, 2011; Wang et al., 2014a; Chen et al., 2015; Chiang and Friedman, 2012; Clemens et al., 2021). Given the amplification of the precessional signal during periods of high eccentricity (Chiang and Broccoli, 2023) (Fig. S57), our investigation focused on the interval spanning 66-133 ka, thus encompassing three complete precessional cycles.

Many proxies' chronology is astronomically tuned to the Northern Hemisphere summer insolation, making them inappropriate to address the asynchronous signals at different latitudes. Here, we utilize the absolute-dated speleothem $\delta^{18}O$ records which were widely used as proxies of precipitation amount, despite the facts that they are somewhat also affected by precipitation-source $\delta^{18}O$ and temperature (Cruz Jr et al., 2005; Lachniet, 2009; Cai et al., 2010) other factors (Dykoski et al., 2005; Lachniet et al., 2005). We synthesize proxies from China (Cheng et al., 2016), Malaysia (Carolin et al., 2013, 2016) and Brazil (Cruz Jr et al., 2005) to validate our hypothesis (Fig. 12). These records are selected because they are representative of three typical regions (i.e., northern limit, equator and southern limit of low-latitude) and have continuous long coverage and high-resolution Uranium-Thorium chronologies. Moreover, these records also well document the precessional dominated precipitation variations.

Speleothem records are seasonally-biased towards typically biased toward their growing seasons, which are usually the rainy seasons (Kwiecien et al., 2022; Liu et al., 2022). Modern observations indicate that the rainy season near the Chinese proxies southeast China is boreal summer, whereas the dominant rainy season in Brazil is boreal winter. In the vicinity of Malaysia, there are two prevailing rainy seasons, namely the boreal spring and autumn (Fig. S1). Accordingly, we expect that the $\delta^{18}O$ signals in the selected regions reflect precipitation changes in their corresponding rainy seasons.

As depicted in Fig. 1b, the latitude of perihelion reaches its northernmost position at 90° precessional phase (Fig. 1b2b, dashed line, and Fig. 2-3 and S2b), corresponding to maximum insolation in boreal summer and maximum in Eastern Asian summer precipitation. Around the precessional phase of 180° , the latitude of perihelion is close to the equator, corresponding to maximum insolation in autumnal equinox (Fig. 2-3 and S2c). The maximum boreal autumn insolation drives the maximum equatorial precipitation, as evidenced by the speleothem record from Malaysia around 121.7 ka and 99.9 ka (Fig. 1e). When 2c). As perihelion migrates to its southernmost position, i.e., at precessional phase 270° (Fig. 2-3 and S2d), the precipitation optimum is identified in Brazil, in agreement with the boreal winter insolation maxima (Fig. 1d2d). At a precessional phase of 0° , perihelion occurs around the equator in spring equinox (Fig. 2-3 and S2a). This leads to maximal insolation in March (Fig. 1e2c, grey line). We find maximum precipitation signals in the Malaysia speleothem record (Fig. 1e2c, red line) around 110.9 and 88.5 ka, corresponding to two maxima in March insolation. The perihelion moves to its northernmost position at precessional phase of 90° , thus completing a full precessional cycle. We For the East Asian and the South American summer monsoons, they reach their minima during the seasonal insolation minima. In contrast, at the equator, the minimum precipitation occurs not during seasonal insolation minima but during the time when insolation is relatively weak in both rainy seasons, i.e., at the precession phases of 90° and 270° (Fig. 6c), approximately 116.2, 105.5, and 82.8 ka (Fig. 2c).

Regionally, there are not perfect agreements between the seasonal insolation variations and speleothem records. For example, the Chinese proxies peak at 90° longitude of perihelion around 127.3 ka. It stays high until after 121.7 ka. This long-term precipitation optimum was likely maintained by relatively high CO₂ during the last interglacial period. Moreover, millennial-scale abrupt climate changes originating from the North Atlantic also play a role in shaping the precipitation across the low-latitudes (Wang et al., 2008; Chiang and Friedman, 2012). This is evident in the abrupt jumps in $\delta^{18}O$ signals from all different latitudes (Fig. 2). In addition, we noticed that the manifestation of October insolation in the half precessional signals in the Malaysia record is relatively stronger than that of the insolation in March. This is likely attributed to a stronger boreal autumn rain than the boreal spring rain in Malaysia (Fig. S1).

The results based on the speleothem records ~~again~~ suggest that wherever the perihelion occurs, the local terrestrial precipitation peaks. This exhibits an asynchronous precipitation ~~maxima~~ optimum following the meridional migration of perihelion (Fig. 1, dashed line). Near the equator, half-precessional signals are identified, in agreement with our model simulations (Fig. 56) and many other records from the tropical area (Trauth and Strecker, 1996; Trauth et al., 2003; Verschuren et al., 2009; Jian et al., 2020).

It is interesting to note that shifting perihelion causes changes in the rainy seasons. ~~Earlier~~ An earlier study found that the shift of maximum summer insolation ~~have~~ has a strong impact on the Asian monsoon (Braconnot and Marti, 2003). Boreal spring perihelion leads early northward migration of the Northern Hemisphere westerly jet (Wu et al., 2023a). In our simulations, we ~~identified that the rainy season can shift~~ identify that the dominant rainy season shifted from June to September near the 10°N latitudinal belt. At the equator, the dominant rainy season switches from April to October following the shift in perihelion (Fig. 56). This could complicate the comparison between proxies and models, as variations in the rainy seasons ~~cannot be distinguished~~ are difficult to distinguish by proxies (Kwiecien et al., 2022).

7 Discussions and Conclusion

In this study, we investigate the dynamics of asynchronous evolution of low-latitude precipitation under precession forcing, a long-standing conundrum in paleoclimate research. We hypothesize that the precessional-scale low-latitude hydrological cycle is paced by shifting perihelion rather than the hemispheric summer insolation. Using two sets of idealized climate model simulations, we showed that whenever and wherever perihelion occurs, the tropical terrestrial precipitation peaks in the corresponding perihelion season and latitudinal band. Under this new framework, the low-latitude precipitation naturally follows distinct rhythms. Speleothem proxies from three typical latitudes were included to test our hypothesis, which shows that the regional precipitation optimum matches the meridional migration of perihelion latitude.

~~Many transient simulations have been conducted~~ Previous studies have used transient simulations to investigate the dynamics of orbital-scale climate changes. These simulations introduced transient forcing attributed to changing Earth's orbit (Kutzbach et al., 2008; He, 2011; Liu et al., 2022) (Kutzbach et al., 2008; He, 2011; Singarayer et al., 2017; Liu et al., 2022), CO₂, land-sea mask, and ice-sheet configurations (Liu et al., 2009). Despite ~~been being~~ more realistic, the simulations with various forcing factors have added difficulty to ~~disentangle~~ disentangling the dynamics of precession's impact on low-latitude climate

340 changes (Chen et al., 2015; Cheng et al., 2021; Griffiths et al., 2009; Ran and Feng, 2013). Time-slice simulations with precession extremes were also performed (Kutzbach, 1981; Braconnot et al., 2008; Battisti et al., 2014; Erb et al., 2015; Bosmans et al., 2018; Jaliha et al., 2019) to assess the precession's role in climate change. However, they are unable to capture the diverse evolution patterns of low-latitude precipitation, as revealed by proxies (An et al., 2000; Wang et al., 2004; Cruz Jr et al., 2005; Cheng et al., 2013; Carolin et al., 2013, 2016; Zhou et al., 2022). In this study, we performed simulations purely
345 forced by a varying precessional phase. The results reveal that the low-latitude terrestrial precipitation maxima ~~follows~~follow a shifting perihelion, with a time lag of 1-2 months.

Traditionally, low-latitude precipitation was regarded as a manifestation of global monsoon, which is usually defined as occurring in hemispheric summer (Wang and Ding, 2008; Wang et al., 2014a, 2017; Geen et al., 2020). Therefore, the inter-hemispheric summer insolation difference was considered as the main driver of precipitation changes at ~~low-latitudes~~low
350 latitudes (Wang et al., 2014a; Schneider et al., 2014). Under this framework, the non-summer precipitation has received less attention. In reality, the ~~ITCZ-related~~ITCZ-related precipitation occurs in different seasons (Fig. S34), not ~~necessary~~necessarily during the hemispheric summer. Therefore, a comprehensive hypothesis should explain precipitation changes not only in the hemispheric summer ~~,but also that~~but also in other seasons. We find that shifting perihelion likely plays ~~a more~~an important role in the fluctuations of seasonal and latitudinal tropical precipitation.

355 Several studies have shown that the distance effect, or perihelion and aphelion, has an impact on low-latitude seasonality in addition to the ~~Sun's zenith point march~~march of Earth's subsolar point (Braconnot et al., 2008; Chiang et al., 2022; Beaufort and Sarr, 2023; Wu et al., 2023a; Chiang and Broccoli, 2023; Hunt et al., 2023). Increased solar radiation can thermodynamically shift the tropical convergence zone from ocean to land (Battisti et al., 2014), thus the terrestrial precipitation is enhanced ~~when perihelion occurs at~~perihelion. Perihelion occurs in different seasons and latitudes, driving enhancement of terrestrial
360 precipitation in the corresponding seasons and latitudes. From this point of view, insolation in individual ~~season~~seasons is equally important in determining the evolution of low-latitude precipitation.

Astronomical tuning is widely used to establish the chronology of paleo proxies. By doing this, the phasing of proxies is artificially synchronized. However, our results indicate that the astronomically driven climate changes can naturally follow diverse rhythms. This questions the reliability of the astronomical tuning strategy, at least for the ~~low-latitudes~~low-latitude
365 area.

We ~~interpreted~~evaluated our hypothesis using limited speleothem $\delta^{18}O$ records as proxies of the precipitation amount. However, speleothem $\delta^{18}O$ signals can be influenced not only by changes in precipitation amount but also by a variety of other factors (Baker et al., 2019), such as the moisture source (Maher and Thompson, 2012), the transport pathway (Griffiths et al., 2009; Wurtze
370 , the degree of upstream precipitation (Cheng et al., 2013; Shi et al., 2025), atmospheric circulation (Breitenbach et al., 2010; Sinha et al., 2019), cave microclimate (Treble et al., 2022; Patterson et al., 2024), or a combination of these processes (Dykoski et al., 2005; Lachniet, 2009; F
. This causes additional uncertainties. Therefore, validating using a wide range of additional proxies is necessary and welcomed.

The present study focuses solely on how precession affects the low-latitude hydrological cycle. ~~Meanwhile, sensitivity simulations indicate that changing obliquity, greenhouse gas concentrations, ice sheets (Weber and Tuenter, 2011; Wang et al., 2014a; Chen~~

375 ~~and millennial-scale Dansgaard-Oeschger events (Chiang and Friedman, 2012) all affect the ITCZ and low-latitude~~ Besides
precession, many other factors also contribute to shaping the ITCZ precipitation. For example, ~~increased obliquity enhances~~
~~high obliquity increases~~ the hemispheric summer insolation, ~~therefore, contribute to increasing the terrestrial precipitation~~
~~in the hemispheric summer (Erb et al., 2015; Bosmans et al., 2018).~~ The combination of different forcings can lead thereby
contributing to an increase in hemispheric monsoon precipitation (Erb et al., 2015; Bischoff et al., 2017; Bosmans et al., 2018)
380 . The presence of high-latitude ice sheets introduces hemispheric cooling, moving the ITCZ away from the cold hemisphere
(Chiang and Bitz, 2005; Weber and Tuenter, 2011; Chen et al., 2015; Clemens et al., 2021; Wu et al., 2023b). Similarly, abrupt
North Atlantic cooling events associated with the collapse of the Atlantic Meridional Overturning Circulation drive the
southward shift of the ITCZ (Wang et al., 2008; Chiang and Friedman, 2012; Singarayer et al., 2017). Sea level fluctuations
alter the land-sea distribution, affecting the supply of moisture, and therefore regional precipitation (Griffiths et al., 2009). The
385 combination of these factors results in a complex evolution of precipitation changes ~~, as recorded in proxies (Carolin et al., 2013; Yuan et al.,~~
(Bischoff et al., 2017; Lyu et al., 2021; Yuan et al., 2023), which may also give rise to asynchronous precipitation signals throughout
low-latitude regions.

By detailing the position and seasonal timing of perihelion (Fig. 23), the precession-induced terrestrial precipitation maxima
can be easily predicted at a given latitude and season. Currently, perihelion takes place around the Tropic of Capricorn, the
390 southern hemisphere summer monsoon is relatively strong. Over the next few thousand years, following the movement of
perihelion towards the equator, the equatorial terrestrial precipitation around the spring equinox will be enhanced. Compared
to the classical theory, which highlights the role of summer insolation, ~~our hypothesis provides a more comprehensive and~~
~~in driving a synchronous ITCZ migration, we hypothesize an asynchronous nature of low-latitude precipitation optimums~~
~~following the shifting perihelion. This offers a more~~ plausible explanation for the observed asynchronous pattern of low-
395 latitude precipitation ~~variations raised from~~ 's response to precessional forcing.

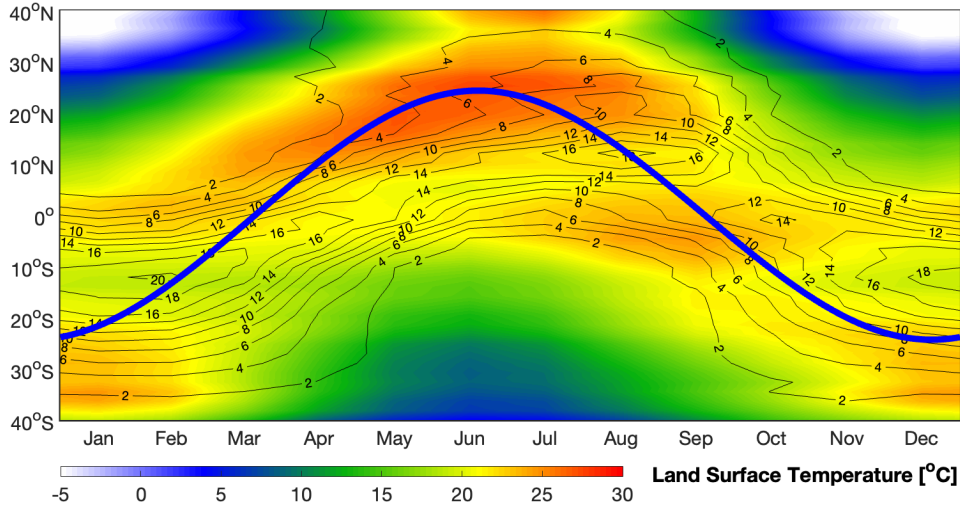


Figure 1. Seasonal migration of the Earth's subsolar point (athick blue line) Climatology map of annual mean precipitation, thermal equator over low-latitudes. Stalagmite oxygen isotope evolution in land (bshading color) China (Cheng et al., 2016) (c) Malaysia (4.1°N; 114.9°E) (Carolin et al., 2013, 2016) and precipitation over land (dblack contours) Brazil. Shading colors represent zonal mean land surface temperature. Contours show the zonal mean precipitation on land (27°-13°-24° S, 49°-09°-20° W) unit: mm/day) (Cruz Jr et al., 2005). The locations-seasonal movement of these records are shown in Fig. 1a. The intensity the Earth's subsolar point fundamentally determines the position of solar radiation in the rainy seasons are plotted as well: for China Earth's thermal equator, it is the averaged solar radiation in June where deep convection and July; for Malaysia low-latitude precipitation takes place. Due to the thermal inertia of Earth, it is the solar radiation in October thermal equator and March; for Brazil, it is land precipitation do not precisely coincide with the mean-timing of maximal solar radiation in January and February. The dashed line illustrates, i.e., the latitude Earth's subsolar point, but rather experience a delay of perihelion (see detailed definition in section 2) approximately 1-2 months. To better illustrate Results are based on the terrestrial precipitation optimums at ensemble mean of the 24 simulations with different precessional phases, we translate the age into precessional phase, which is shown in the upper axis (see Methodology). When the perihelion passes certain latitude, the seasonal solar radiation and terrestrial precipitation reach their maxima.

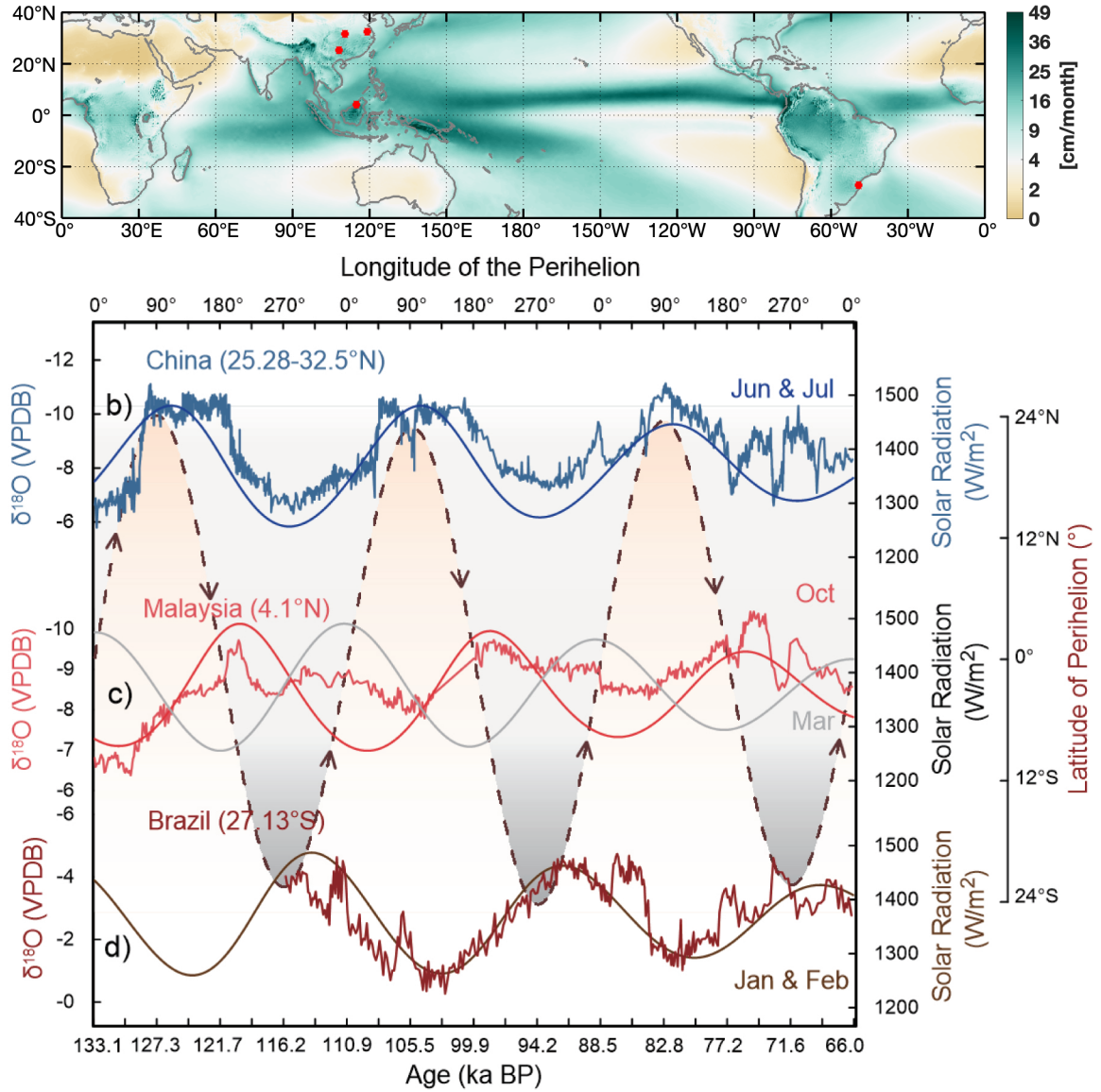


Figure 2. (a) Climatology map of annual mean precipitation over low-latitudes. Stalagmite oxygen isotope evolution in (b) China (Cheng et al., 2016) (c) Malaysia (4.1°N, 114.9°E) (Carolin et al., 2013, 2016) and (d) Brazil (27°13' 24" S, 49°09' 20" W) (Cruz Jr et al., 2005). The locations of these records are shown in Fig. 2a. The intensity of solar radiation in the rainy seasons are plotted as well: for China, it is the averaged solar radiation in June and July; for Malaysia, it is the solar radiation in October and March; for Brazil, it is the mean solar radiation in January and February. The dashed line illustrates the meridional migration of perihelion latitude (see detailed definition in Section 3). To better illustrate the terrestrial precipitation optimums at different precessional phases, we translate the age into precessional phase, which is shown in the upper axis. When the perihelion passes certain latitude, the seasonal solar radiation and terrestrial precipitation reach their maxima.

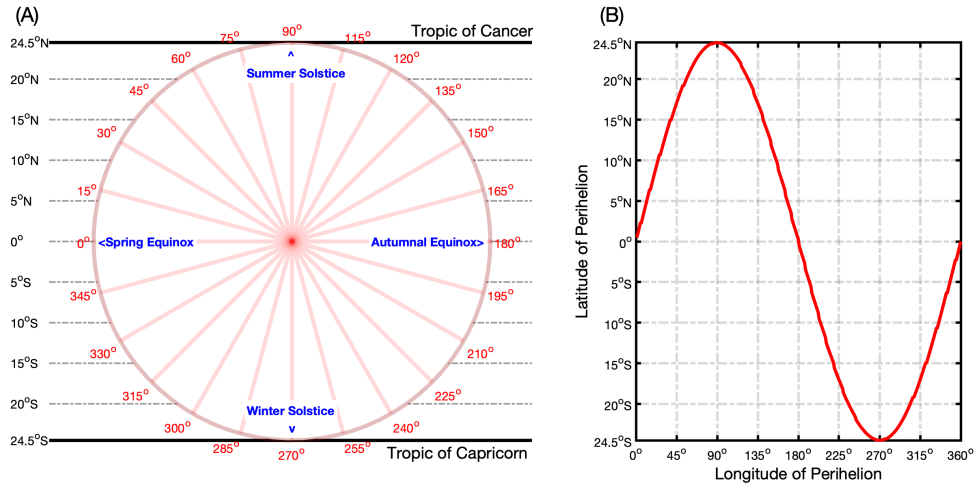


Figure 3. The latitudinal movement of the perihelion and ~~Sun-Earth's zenith-subsolar~~ point within a precessional cycle and an annual cycle, respectively. The labels outside the circle give the precessional phase, namely the longitude of the perihelion. The labels inside the circle locate the position of season. Within a year, the ~~Sun-Earth's zenith-subsolar~~ point march between the Tropic of Cancer and the Tropic of Capricorn. Within a precessional cycle, the latitude of perihelion also migrates between the Tropic of Cancer and the Tropic of Capricorn. The grey dashed lines give the latitudinal coordinate. When the perihelion occurs, the insolation at the perihelion latitude reaches the maximum within a precessional cycle. To better understand this figure, please also check Supplementary Movie 1 (<https://zenodo.org/doi/10.5281/zenodo.11395458>), which visually conveys an explanatory description of the seasonal solar radiation variations within a precessional cycle.

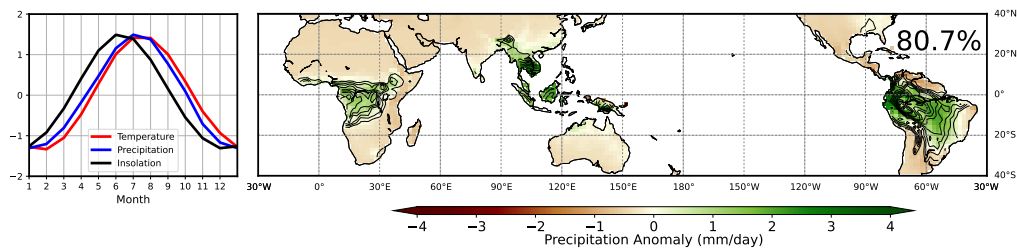


Figure 4. Temporal and spatial evolutions of terrestrial precipitation in the idealised Earth system experiment, with zero obliquity and high eccentricity (0.058). The shading color in the right panel illustrates the spatial pattern of the leading mode (contains 80.7% of terrestrial precipitation covariance) of Empirical Orthogonal Function (EOF) analysis on the monthly convective precipitation over land. The contours illustrate the climatology precipitation. The blue lines in the left panels show the corresponding principal component, illustrating the temporal evolution of the terrestrial precipitation strength. The area-weighted land-surface temperature (red line) and incoming solar radiation (black line) evolution are plotted as well. In this experiment, perihelion occurs in June, corresponding to maximum incoming solar radiation in June and maximum precipitation over land 1-2 month later (July and August).

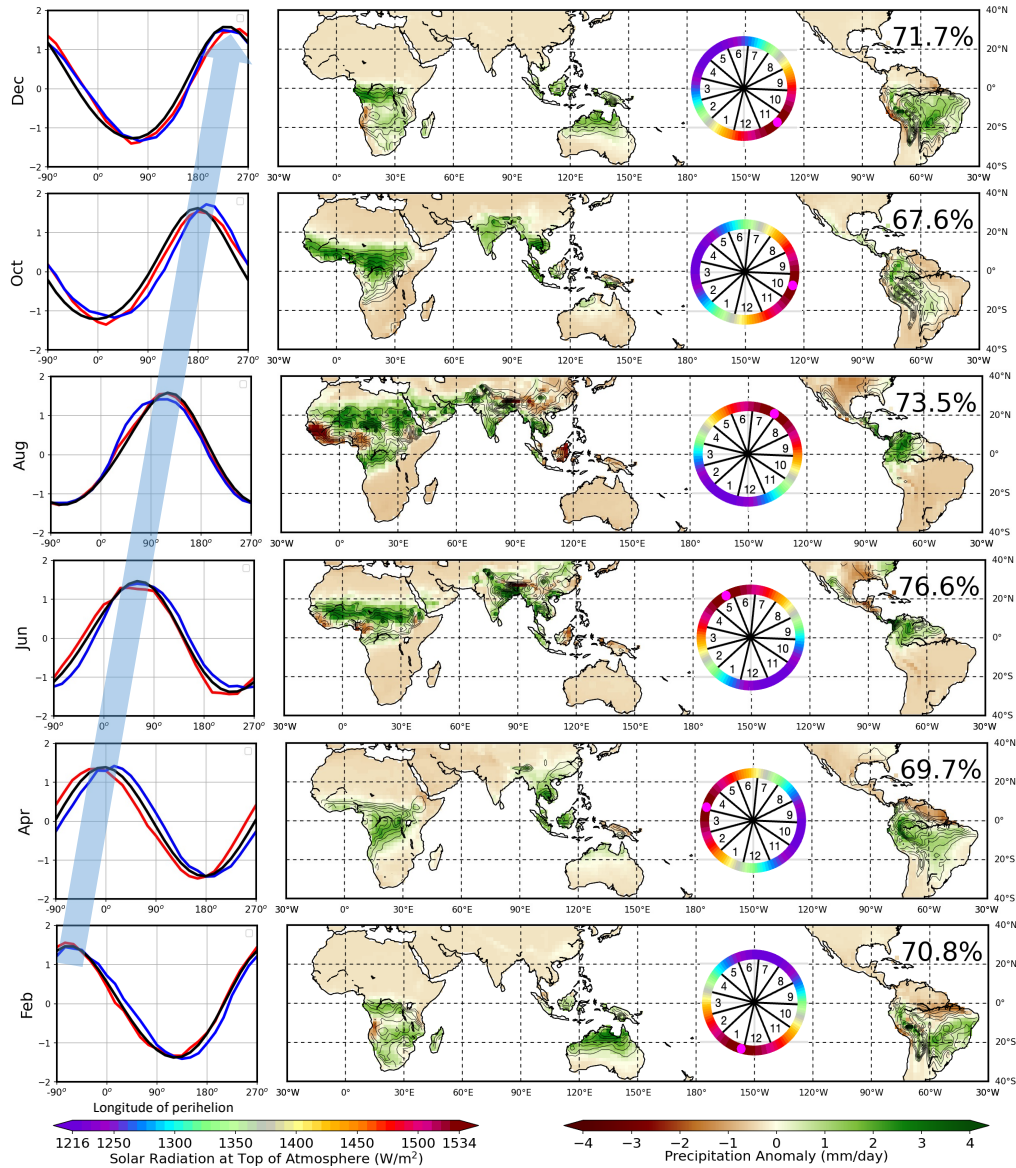


Figure 5. Temporal and spatial evolutions of terrestrial precipitation in different seasons. The shading color in the right panel illustrates the spatial pattern of the leading mode of Empirical Orthogonal Function (EOF) analysis on the monthly terrestrial precipitation simulated by AWI-ESM recovering a precessional cycle. The numbers in the subpanels' upper-right corner displays the contribution of the first principal component of EOF to the overall variance. The contours illustrate the climatology precipitation [in the corresponding month](#). The blue lines in the left panels show the corresponding principal component [of EOF analysis](#), illustrating the temporal evolution of the terrestrial precipitation strength. The area-weighted land-surface temperature (red line) and incoming solar radiation (black line) evolution are plotted as well. Note that, the plotted solar radiation is from an earlier month. For example, for the panel of February, the solar radiation in January is plotted. For comparison, all time-series are normalised. The colored circles illustrate the solar radiation distribution when the corresponding seasonal terrestrial precipitation peaks. The numbers in this circle give the location of the individual month. The pink dots give the timing and meridional position of perihelion. The blue [patches illustrate arrow in the approximate location of left panels illustrates the thermal-equator asynchronous precipitation optimums across different latitudes and rain-belt-on-land seasons](#).

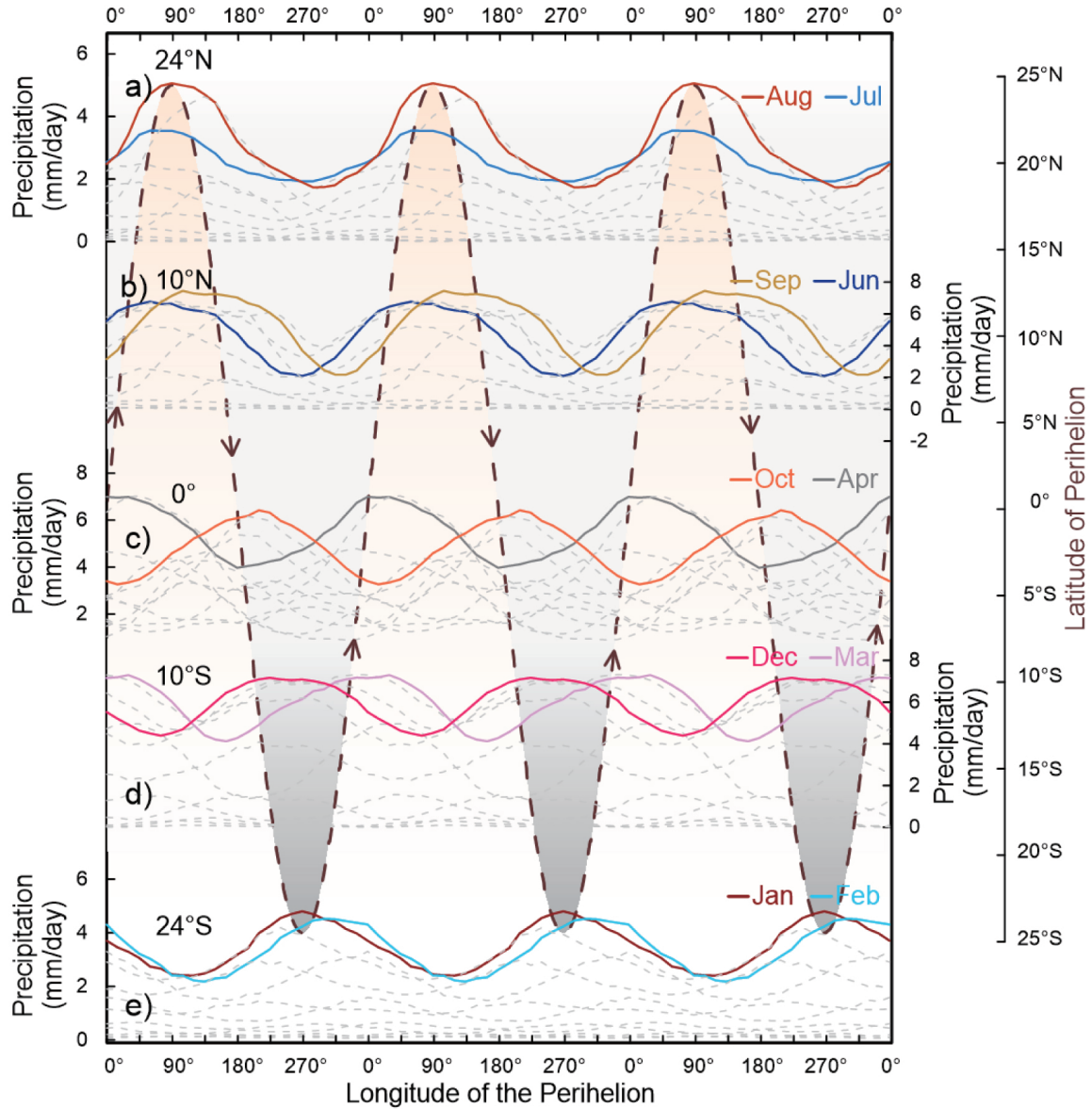


Figure 6. The simulated evolution of monthly precipitation at different latitudinal bands over three precessional cycles. The precipitation is calculated as zonal mean terrestrial precipitation over latitudinal bands covering a width of five degrees. For each latitudinal band, the rainy seasons are highlighted with colored lines, and precipitation in other months is shown as grey dashed lines. The dashed copper line illustrates the meridional movement of Earth's perihelion between the Tropic of Cancer and the Tropic of Capricorn, namely the latitude of perihelion. Whenever (the season) and wherever (the latitude) perihelion occurs, the local terrestrial precipitation in the corresponding month reaches its maximum within a precessional cycle.

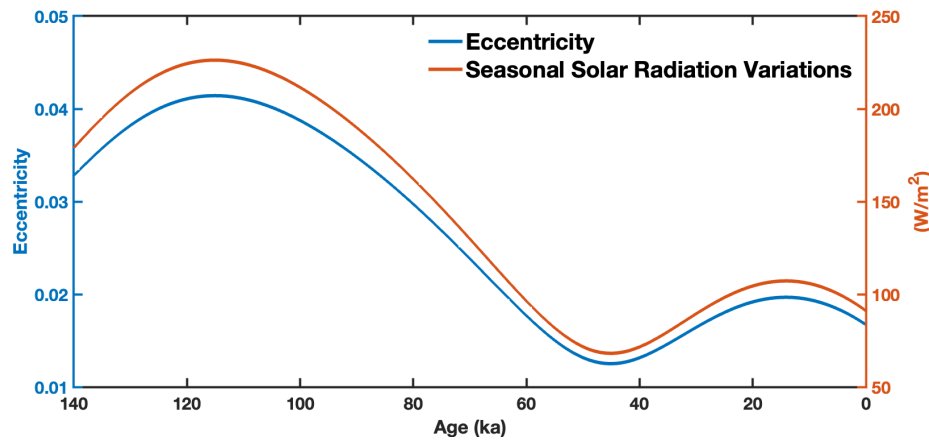


Figure 7. Eccentricity and magnitude of seasonal variations in solar radiation intensity over the past 140 ka. The eccentricity is calculated according to Berger (1978), and the amplitude of seasonal incoming solar radiation intensity is computed as the difference between the solar radiation at perihelion and aphelion.

Data availability. The model output used in this study can be accessed from <https://zenodo.org/doi/10.5281/zenodo.13681175>.

Author contributions. H. Yang conceived the idea and wrote the first draft. All authors participated in the manuscript's discussion and revision.

Competing interests. The authors have declared that no competing interests exist.

400 *Acknowledgements.* We acknowledge Marie-France Loutre and the other two reviewers for providing valuable comments to improve the manuscript. The study was supported by ~~the construction fund of the Frontier Research Center at the~~ Southern Marine Science and Engineering Guangdong Laboratory (Zhuhai), No. SML2023SP204, ~~and fund from~~ the Ocean Negative Carbon Emissions (ONCE) Program and the National Natural Science Foundation of China. The AWI-ESM simulations were conducted on Deutsche Klimarechenzentrum (DKRZ) and AWI supercomputer (Ollie).

- An, Z., Porter, S. C., Kutzbach, J. E., Xihao, W., Suming, W., Xiaodong, L., Xiaoqiang, L., and Weijian, Z.: Asynchronous Holocene optimum of the East Asian monsoon, *Quaternary Science Reviews*, 19, 743–762, 2000.
- Armstrong, E., Tallavaara, M., Hopcroft, P. O., and Valdes, P. J.: North African humid periods over the past 800,000 years, *Nature Communications*, 14, 5549, 2023.
- 410 Baker, A., Hartmann, A., Duan, W., Hankin, S., Comas-Bru, L., Cuthbert, M. O., Treble, P. C., Banner, J., Genty, D., Baldini, L. M., et al.: Global analysis reveals climatic controls on the oxygen isotope composition of cave drip water, *Nature Communications*, 10, 2984, 2019.
- Baker, P. A., Rigsby, C. A., Seltzer, G. O., Fritz, S. C., Lowenstein, T. K., Bacher, N. P., and Veliz, C.: Tropical climate changes at millennial and orbital timescales on the Bolivian Altiplano, *nature*, 409, 698–701, 2001.
- Barry, R. G. and Chorley, R. J.: *Atmosphere, weather and climate*, Routledge, 2009.
- 415 Battisti, D., Ding, Q., and Roe, G.: Coherent pan-Asian climatic and isotopic response to orbital forcing of tropical insolation, *Journal of Geophysical Research: Atmospheres*, 119, 11–997, 2014.
- Beaufort, L. and Sarr, A. C.: Eccentricity forcing on Tropical Ocean Seasonality, *Climate of the Past Discussions*, 2023, 1–32, 2023.
- Beaufort, L., Van der Kaars, S., Bassinot, F., and Moron, V.: Past dynamics of the Australian monsoon: precession, phase and links to the global monsoon concept, *Climate of the Past*, 6, 695–706, 2010.
- 420 Berger, A.: Long-term variations of daily insolation and Quaternary climatic changes, *Journal of Atmospheric Sciences*, 35, 2362–2367, 1978.
- Berger, A.: Milankovitch theory and climate, *Reviews of geophysics*, 26, 624–657, 1988.
- Bischoff, T., Schneider, T., and Meckler, A. N.: A conceptual model for the response of tropical rainfall to orbital variations, *Journal of Climate*, 30, 8375–8391, 2017.
- 425 Bosmans, J., Erb, M., Dolan, A., Drijfhout, S., Tuenter, E., Hilgen, F., Edge, D., Pope, J. O., and Lourens, L.: Response of the Asian summer monsoons to idealized precession and obliquity forcing in a set of GCMs, *Quaternary Science Reviews*, 188, 121–135, 2018.
- Braconnot, P. and Marti, O.: Impact of precession on monsoon characteristics from coupled ocean atmosphere experiments: changes in Indian monsoon and Indian ocean climatology, *Marine Geology*, 201, 23–34, 2003.
- Braconnot, P., Marzin, C., Grégoire, L., Mosquet, E., and Marti, O.: Monsoon response to changes in Earth’s orbital parameters: comparisons between simulations of the Eemian and of the Holocene, *Climate of the Past*, 4, 281–294, 2008.
- 430 Breitenbach, S. F., Adkins, J. F., Meyer, H., Marwan, N., Kumar, K. K., and Haug, G. H.: Strong influence of water vapor source dynamics on stable isotopes in precipitation observed in Southern Meghalaya, NE India, *Earth and Planetary Science Letters*, 292, 212–220, 2010.
- Cai, Y., Tan, L., Cheng, H., An, Z., Edwards, R. L., Kelly, M. J., Kong, X., and Wang, X.: The variation of summer monsoon precipitation in central China since the last deglaciation, *Earth and Planetary Science Letters*, 291, 21–31, 2010.
- 435 Carolin, S. A., Cobb, K. M., Adkins, J. F., Clark, B., Conroy, J. L., Lejau, S., Malang, J., and Tuen, A. A.: Varied response of western Pacific hydrology to climate forcings over the last glacial period, *Science*, 340, 1564–1566, 2013.
- Carolin, S. A., Cobb, K. M., Lynch-Stieglitz, J., Moerman, J. W., Partin, J. W., Lejau, S., Malang, J., Clark, B., Tuen, A. A., and Adkins, J. F.: Northern Borneo stalagmite records reveal West Pacific hydroclimate across MIS 5 and 6, *Earth and Planetary Science Letters*, 439, 182–193, 2016.
- 440 Chen, F., Xu, Q., Chen, J., Birks, H. J. B., Liu, J., Zhang, S., Jin, L., An, C., Telford, R. J., Cao, X., et al.: East Asian summer monsoon precipitation variability since the last deglaciation, *Scientific reports*, 5, 1–11, 2015.

- Cheng, H., Edwards, R. L., Broecker, W. S., Denton, G. H., Kong, X., Wang, Y., Zhang, R., and Wang, X.: Ice age terminations, *science*, 326, 248–252, 2009.
- Cheng, H., Sinha, A., Wang, X., Cruz, F. W., and Edwards, R. L.: The Global Paleomonsoon as seen through speleothem records from Asia
445 and the Americas, *Climate dynamics*, 39, 1045–1062, 2012.
- Cheng, H., Sinha, A., Cruz, F. W., Wang, X., Edwards, R. L., d'Horta, F. M., Ribas, C. C., Vuille, M., Stott, L. D., and Auler, A. S.: Climate change patterns in Amazonia and biodiversity, *Nature communications*, 4, 1411, 2013.
- Cheng, H., Edwards, R. L., Sinha, A., Spötl, C., Yi, L., Chen, S., Kelly, M., Kathayat, G., Wang, X., Li, X., et al.: The Asian monsoon over the past 640,000 years and ice age terminations, *nature*, 534, 640–646, 2016.
- 450 Cheng, H., Li, H., Sha, L., Sinha, A., Shi, Z., Yin, Q., Lu, Z., Zhao, D., Cai, Y., Hu, Y., et al.: Milankovitch theory and monsoon, *The Innovation*, 3, 2022.
- Cheng, J., Wu, H., Liu, Z., Gu, P., Wang, J., Zhao, C., Li, Q., Chen, H., Lu, H., Hu, H., et al.: Vegetation feedback causes delayed ecosystem response to East Asian Summer Monsoon Rainfall during the Holocene, *Nature Communications*, 12, 1843, 2021.
- Chiang, J. C. and Bitz, C. M.: Influence of high latitude ice cover on the marine Intertropical Convergence Zone, *Climate Dynamics*, 25,
455 477–496, 2005.
- Chiang, J. C. and Broccoli, A. J.: A role for orbital eccentricity in Earth's seasonal climate, *Geoscience Letters*, 10, 58, 2023.
- Chiang, J. C. and Friedman, A. R.: Extratropical cooling, interhemispheric thermal gradients, and tropical climate change, *Annual Review of Earth and Planetary Sciences*, 40, 383–412, 2012.
- Chiang, J. C., Atwood, A. R., Vimont, D. J., Nicknisch, P. A., Roberts, W. H., Tabor, C. R., and Broccoli, A. J.: Two annual cycles of the
460 Pacific cold tongue under orbital precession, *Nature*, 611, 295–300, 2022.
- Clemens, S. C. and Prell, W. L.: The timing of orbital-scale Indian monsoon changes, *Quaternary Science Reviews*, 26, 275–278, 2007.
- Clemens, S. C., Yamamoto, M., Thirumalai, K., Giosan, L., Richey, J. N., Nilsson-Kerr, K., Rosenthal, Y., Anand, P., and McGrath, S. M.: Remote and local drivers of Pleistocene South Asian summer monsoon precipitation: A test for future predictions, *Science Advances*, 7, eabg3848, 2021.
- 465 Clement, A. C., Hall, A., and Broccoli, A.: The importance of precessional signals in the tropical climate, *Climate dynamics*, 22, 327–341, 2004.
- Cruz Jr, F. W., Burns, S. J., Karmann, I., Sharp, W. D., Vuille, M., Cardoso, A. O., Ferrari, J. A., Silva Dias, P. L., and Viana Jr, O.: Insolation-driven changes in atmospheric circulation over the past 116,000 years in subtropical Brazil, *Nature*, 434, 63–66, 2005.
- Danilov, S., Sidorenko, D., Wang, Q., and Jung, T.: The finite-volume sea ice–ocean model (fesom2), *Geoscientific Model Development*, 10,
470 765–789, 2017.
- DeMenocal, P. B., Tierney, J. E., et al.: Green Sahara: African humid periods paced by Earth's orbital changes, *Nature Education Knowledge*, 3, 12, 2012.
- Donohoe, A., Dawson, E., McMurdie, L., Battisti, D. S., and Rhines, A.: Seasonal asymmetries in the lag between insolation and surface temperature, *Journal of Climate*, 33, 3921–3945, 2020.
- 475 Dykoski, C. A., Edwards, R. L., Cheng, H., Yuan, D., Cai, Y., Zhang, M., Lin, Y., Qing, J., An, Z., and Revenaugh, J.: A high-resolution, absolute-dated Holocene and deglacial Asian monsoon record from Dongge Cave, China, *Earth and Planetary Science Letters*, 233, 71–86, 2005.
- El-Shenawy, M. I., Kim, S.-T., Schwarcz, H. P., Asmerom, Y., and Polyak, V. J.: Speleothem evidence for the greening of the Sahara and its implications for the early human dispersal out of sub-Saharan Africa, *Quaternary Science Reviews*, 188, 67–76, 2018.

- 480 Erb, M. P., Jackson, C. S., and Broccoli, A. J.: Using single-forcing GCM simulations to reconstruct and interpret quaternary climate change, *Journal of climate*, 28, 9746–9767, 2015.
- Fairchild, I. J. and Baker, A.: *Speleothem science: from process to past environments*, John Wiley & Sons, 2012.
- Gadgil, S.: The monsoon system: Land–sea breeze or the ITCZ?, *Journal of Earth System Science*, 127, 1–29, 2018.
- Geen, R., Bordoni, S., Battisti, D. S., and Hui, K.: Monsoons, ITCZs, and the concept of the global monsoon, *Reviews of Geophysics*, 58,
485 e2020RG000700, 2020.
- Giorgetta, M. A., Roeckner, E., Mauritsen, T., Bader, J., Crueger, T., Esch, M., Rast, S., Kornblueh, L., Schmidt, H., Kinne, S., et al.: The atmospheric general circulation model ECHAM6-model description, 2013.
- Griffiths, M. L., Drysdale, R. N., Gagan, M., Zhao, J.-x., Ayliffe, L., Hellstrom, J. C., Hantoro, W., Frisia, S., Feng, Y.-x., Cartwright, I., et al.: Increasing Australian–Indonesian monsoon rainfall linked to early Holocene sea-level rise, *Nature Geoscience*, 2, 636–639, 2009.
- 490 Hannachi, A., Jolliffe, I. T., Stephenson, D. B., et al.: Empirical orthogonal functions and related techniques in atmospheric science: A review, *International journal of climatology*, 27, 1119–1152, 2007.
- He, F.: *Simulating transient climate evolution of the last deglaciation with CCSM 3*, vol. 72, University of Wisconsin–Madison, 2011.
- Hély, C., Lézine, A.-M., et al.: Holocene changes in African vegetation: tradeoff between climate and water availability, *Climate of the Past*, 10, 681–686, 2014.
- 495 Hunt, J., Lister, K., Nascimento, A., and Vasconcelos de Freitas, M.: The Ideal Climate Latitude: Orbit and Axial Precession Influence in Ancient Migration, *Archaeology & Anthropology: Open Access*, 4, 671–678, 2023.
- Jalihal, C., Bosmans, J. H. C., Srinivasan, J., and Chakraborty, A.: The response of tropical precipitation to Earth’s precession: the role of energy fluxes and vertical stability, *Climate of the Past*, 15, 449–462, 2019.
- Jian, Z., Wang, Y., Dang, H., Lea, D. W., Liu, Z., Jin, H., and Yin, Y.: Half-precessional cycle of thermocline temperature in the western equatorial Pacific and its bihemispheric dynamics, *Proceedings of the National Academy of Sciences*, 117, 7044–7051, 2020.
- 500 Joussaume, S. and Braconnot, P.: Sensitivity of paleoclimate simulation results to season definitions, *Journal of Geophysical Research: Atmospheres*, 102, 1943–1956, 1997.
- Kageyama, M., Braconnot, P., Harrison, S. P., Haywood, A. M., Jungclaus, J. H., Otto-Bliesner, B. L., Peterschmitt, J.-Y., Abe-Ouchi, A., Albani, S., Bartlein, P. J., et al.: The PMIP4 contribution to CMIP6–Part 1: Overview and over-arching analysis plan, *Geoscientific Model Development*, 11, 1033–1057, 2018.
- 505 Kaushal, N., Lechleitner, F. A., Wilhelm, M., Azennoud, K., Bühler, J. C., Braun, K., Ait Brahim, Y., Baker, A., Burstyn, Y., Comas-Bru, L., et al.: SISALv3: a global speleothem stable isotope and trace element database, *Earth system science data*, 16, 1933–1963, 2024.
- Kelly, M. J., Edwards, R. L., Cheng, H., Yuan, D., Cai, Y., Zhang, M., Lin, Y., and An, Z.: High resolution characterization of the Asian Monsoon between 146,000 and 99,000 years BP from Dongge Cave, China and global correlation of events surrounding Termination II, *Palaeogeography, Palaeoclimatology, Palaeoecology*, 236, 20–38, 2006.
- 510 Kostadinov, T. and Gilb, R.: *Earth Orbit v2. 1: a 3-D visualization and analysis model of Earth’s orbit, Milankovitch cycles and insolation*, *Geoscientific Model Development*, 7, 1051–1068, 2014.
- Kuper, R. and Kropelin, S.: Climate-controlled Holocene occupation in the Sahara: motor of Africa’s evolution, *science*, 313, 803–807, 2006.
- Kutzbach, J. and Gallimore, R.: Sensitivity of a coupled atmosphere/mixed layer ocean model to changes in orbital forcing at 9000 years BP, *Journal of Geophysical Research: Atmospheres*, 93, 803–821, 1988.
- 515 Kutzbach, J., Liu, X., Liu, Z., and Chen, G.: Simulation of the evolutionary response of global summer monsoons to orbital forcing over the past 280,000 years, *Climate Dynamics*, 30, 567–579, 2008.

- Kutzbach, J. E.: Monsoon climate of the early Holocene: climate experiment with the earth's orbital parameters for 9000 years ago, *Science*, 214, 59–61, 1981.
- 520 Kwiecien, O., Braun, T., Brunello, C. F., Faulkner, P., Hausmann, N., Helle, G., Hoggarth, J. A., Ionita, M., Jazwa, C. S., Kelmelis, S., et al.: What we talk about when we talk about seasonality—A transdisciplinary review, *Earth-Science Reviews*, 225, 103 843, 2022.
- Lachniet, M. S.: Climatic and environmental controls on speleothem oxygen-isotope values, *Quaternary Science Reviews*, 28, 412–432, 2009.
- Laskar, J.: The chaotic motion of the solar system: A numerical estimate of the size of the chaotic zones, *Icarus*, 88, 266–291, 1990.
- 525 Laskar, J., Joutel, F., and Boudin, F.: Orbital, precessional, and insolation quantities for the Earth from-20 Myr to+ 10 Myr, *Astronomy and Astrophysics (ISSN 0004-6361)*, vol. 270, no. 1-2, p. 522-533., 270, 522–533, 1993.
- Li, X., Zhou, Y., Han, Z., Yuan, X., Yi, S., Zeng, Y., Qin, L., Lu, M., and Lu, H.: Loess deposits in the low latitudes of East Asia reveal the 20-kyr precipitation cycle, *Nature Communications*, 15, 1023, 2024.
- Lisiecki, L. E. and Raymo, M. E.: A Pliocene-Pleistocene stack of 57 globally distributed benthic $\delta^{18}\text{O}$ records, *Paleoceanography*, 20, 2005.
- 530 Liu, J., Chen, J., Zhang, X., Li, Y., Rao, Z., and Chen, F.: Holocene East Asian summer monsoon records in northern China and their inconsistency with Chinese stalagmite $\delta^{18}\text{O}$ records, *Earth-Science Reviews*, 148, 194–208, 2015.
- Liu, X., Xie, X., Guo, Z., Yin, Z.-Y., and Chen, G.: Model-based orbital-scale precipitation $\delta^{18}\text{O}$ variations and distinct mechanisms in Asian monsoon and arid regions, *National Science Review*, 9, nwac182, 2022.
- Liu, Z., Otto-Bliesner, B., He, F., Brady, E., Tomas, R., Clark, P., Carlson, A., Lynch-Stieglitz, J., Curry, W., Brook, E., et al.: Transient simulation of last deglaciation with a new mechanism for Bølling-Allerød warming, *science*, 325, 310–314, 2009.
- 535 Loughheed, B. C.: Orbital, the Box-An interactive educational tool for in-depth understanding of astronomical climate forcing., 2021.
- Lu, H., Yi, S., Liu, Z., Mason, J. A., Jiang, D., Cheng, J., Stevens, T., Xu, Z., Zhang, E., Jin, L., et al.: Variation of East Asian monsoon precipitation during the past 21 ky and potential CO₂ forcing, *Geology*, 41, 1023–1026, 2013.
- Lyu, A., Yin, Q., Crucifix, M., and Sun, Y.: Diverse regional sensitivity of summer precipitation in East Asia to ice volume, CO₂ and astronomical forcing, *Geophysical Research Letters*, 48, e2020GL092 005, 2021.
- 540 Maher, B. A. and Thompson, R.: Oxygen isotopes from Chinese caves: records not of monsoon rainfall but of circulation regime, *Journal of Quaternary Science*, 27, 615–624, 2012.
- McGrath, S. M., Clemens, S. C., Huang, Y., and Yamamoto, M.: Greenhouse gas and ice volume drive Pleistocene Indian summer monsoon precipitation isotope variability, *Geophysical Research Letters*, 48, e2020GL092 249, 2021.
- 545 Milankovitch, M.: Canon of Insolation and the Ice Age Problem (in German), *Königlich Serbische Akademie*, 1941.
- Neelin, J. D. and Held, I. M.: Modeling tropical convergence based on the moist static energy budget, *Monthly Weather Review*, 115, 3–12, 1987.
- Parker, S. E., Harrison, S. P., Comas-Bru, L., Kaushal, N., LeGrande, A. N., and Werner, M.: A data–model approach to interpreting speleothem oxygen isotope records from monsoon regions, *Climate of the Past*, 17, 1119–1138, 2021.
- 550 Patterson, E., Skiba, V., Wolf, A., Griffiths, M., McGee, D., Bui, T., Tran, M., Dinh, T., Do-Trng, Q., Goldsmith, G. R., et al.: Local hydroclimate alters interpretation of speleothem $\delta^{18}\text{O}$ records, *Nature Communications*, 15, 9064, 2024.
- Pollard, D. and Reusch, D. B.: A calendar conversion method for monthly mean paleoclimate model output with orbital forcing, *Journal of Geophysical Research: Atmospheres*, 107, ACL–3, 2002.
- Ran, M. and Feng, Z.: Holocene moisture variations across China and driving mechanisms: A synthesis of climatic records, *Quaternary International*, 313, 179–193, 2013.
- 555

- Schneider, T., Bischoff, T., and Haug, G. H.: Migrations and dynamics of the intertropical convergence zone, *Nature*, 513, 45–53, 2014.
- Shanahan, T. M., McKay, N. P., Hughen, K. A., Overpeck, J. T., Otto-Bliesner, B., Heil, C. W., King, J., Scholz, C. A., and Peck, J.: The time-transgressive termination of the African Humid Period, *Nature Geoscience*, 8, 140–144, 2015.
- Shi, X. and Lohmann, G.: Simulated response of the mid-Holocene Atlantic meridional overturning circulation in ECHAM6-FESOM/MPIOM, *Journal of Geophysical Research: Oceans*, 121, 6444–6469, 2016.
- Shi, X., Werner, M., Krug, C., Brierley, C. M., Zhao, A., Igbinosa, E., Braconnot, P., Brady, E., Cao, J., d’Agostino, R., et al.: Calendar effects on surface air temperature and precipitation based on model-ensemble equilibrium and transient simulations from PMIP4 and PACMEDY, *Climate of the Past*, 18, 1047–1070, 2022.
- Shi, X., Werner, M., Yang, H., Gao, Q., Liu, J., and Lohmann, G.: Precession controls on climate and water isotope signals in Northern Africa, *Paleoceanography and Paleoclimatology*, 40, e2024PA004999, 2025.
- Short, D. A. and Mengel, J. G.: Tropical climatic phase lags and Earth’s precession cycle, *Nature*, 323, 48–50, 1986.
- Sidorenko, D., Rackow, T., Jung, T., Semmler, T., Barbi, D., Danilov, S., Dethloff, K., Dorn, W., Fieg, K., Gößling, H. F., et al.: Towards multi-resolution global climate modeling with ECHAM6–FESOM. Part I: model formulation and mean climate, *Climate Dynamics*, 44, 757–780, 2015.
- Sidorenko, D., Goessling, H., Koldunov, N., Scholz, P., Danilov, S., Barbi, D., Cabos, W., Gurses, O., Harig, S., Hinrichs, C., et al.: Evaluation of FESOM2.0 coupled to ECHAM6.3: preindustrial and HighResMIP simulations, *Journal of Advances in Modeling Earth Systems*, 11, 3794–3815, 2019.
- Singarayer, J. S., Valdes, P. J., and Roberts, W. H.: Ocean dominated expansion and contraction of the late Quaternary tropical rainbelt, *Scientific reports*, 7, 9382, 2017.
- Sinha, A., Kathayat, G., Cheng, H., Breitenbach, S. F., Berkelhammer, M., Mudelsee, M., Biswas, J., and Edwards, R.: Trends and oscillations in the Indian summer monsoon rainfall over the last two millennia, *Nature communications*, 6, 6309, 2015.
- Sun, Y., Chen, J., Clemens, S. C., Liu, Q., Ji, J., and Tada, R.: East Asian monsoon variability over the last seven glacial cycles recorded by a loess sequence from the northwestern Chinese Loess Plateau, *Geochemistry, Geophysics, Geosystems*, 7, 2006.
- Thamban, M., Kawahata, H., and Rao, V. P.: Indian summer monsoon variability during the Holocene as recorded in sediments of the Arabian Sea: timing and implications, *Journal of oceanography*, 63, 1009–1020, 2007.
- Trauth, M. and Strecker, M.: Late Pleistocene lake-level fluctuations in the Naivasha Basin, Kenya, in: *Limnology, Climatology and Paleoclimatology of the East African Lakes*, pp. 549–557, Routledge, 1996.
- Trauth, M. H., Deino, A. L., Bergner, A. G., and Strecker, M. R.: East African climate change and orbital forcing during the last 175 kyr BP, *Earth and Planetary Science Letters*, 206, 297–313, 2003.
- Treble, P. C., Baker, A., Abram, N. J., Hellstrom, J. C., Crawford, J., Gagan, M. K., Borsato, A., Griffiths, A. D., Bajo, P., Markowska, M., et al.: Ubiquitous karst hydrological control on speleothem oxygen isotope variability in a global study, *Communications Earth & Environment*, 3, 29, 2022.
- Verschuren, D., Sinninghe Damsté, J. S., Moernaut, J., Kristen, I., Blaauw, M., Fagot, M., and Haug, G. H.: Half-precessional dynamics of monsoon rainfall near the East African Equator, *Nature*, 462, 637–641, 2009.
- Wallace, J. M. and Hobbs, P. V.: *Atmospheric science: an introductory survey*, vol. 92, Elsevier, 2006.
- Wang, B. and Ding, Q.: Global monsoon: Dominant mode of annual variation in the tropics, *Dynamics of Atmospheres and Oceans*, 44, 165–183, 2008.

- Wang, P., Wang, B., Cheng, H., Fasullo, J., Guo, Z., Kiefer, T., and Liu, Z.: The global monsoon across timescales: coherent variability of regional monsoons, *Climate of the Past*, 10, 2007–2052, 2014a.
- 595 Wang, P. X., Wang, B., Cheng, H., Fasullo, J., Guo, Z., Kiefer, T., and Liu, Z.: The global monsoon across time scales: Mechanisms and outstanding issues, *Earth-Science Reviews*, 174, 84–121, 2017.
- Wang, Q., Danilov, S., Sidorenko, D., Timmermann, R., Wekerle, C., Wang, X., Jung, T., and Schröter, J.: The Finite Element Sea Ice-Ocean Model (FESOM) v. 1.4: formulation of an ocean general circulation model, *Geoscientific Model Development*, 7, 663–693, 2014b.
- Wang, X., Auler, A. S., Edwards, R. L., Cheng, H., Cristalli, P. S., Smart, P. L., Richards, D. A., and Shen, C.-C.: Wet periods in northeastern
600 Brazil over the past 210 kyr linked to distant climate anomalies, *Nature*, 432, 740–743, 2004.
- Wang, X., Auler, A. S., Edwards, R. L., Cheng, H., Ito, E., and Solheid, M.: Interhemispheric anti-phasing of rainfall during the last glacial period, *Quaternary Science Reviews*, 25, 3391–3403, 2006.
- Wang, X., Auler, A. S., Edwards, R., Cheng, H., Ito, E., Wang, Y., Kong, X., and Solheid, M.: Millennial-scale precipitation changes in southern Brazil over the past 90,000 years, *Geophysical Research Letters*, 34, 2007.
- 605 Wang, Y., Cheng, H., Edwards, R. L., Kong, X., Shao, X., Chen, S., Wu, J., Jiang, X., Wang, X., and An, Z.: Millennial-and orbital-scale changes in the East Asian monsoon over the past 224,000 years, *Nature*, 451, 1090–1093, 2008.
- Wang, Y.-J., Cheng, H., Edwards, R. L., An, Z., Wu, J., Shen, C.-C., and Dorale, J. A.: A high-resolution absolute-dated late Pleistocene monsoon record from Hulu Cave, China, *Science*, 294, 2345–2348, 2001.
- Weber, S. and Tuenter, E.: The impact of varying ice sheets and greenhouse gases on the intensity and timing of boreal summer monsoons,
610 *Quaternary Science Reviews*, 30, 469–479, 2011.
- Windler, G., Tierney, J. E., and Anchukaitis, K. J.: Glacial-interglacial shifts dominate tropical Indo-Pacific hydroclimate during the late Pleistocene, *Geophysical Research Letters*, 48, e2021GL093339, 2021.
- Wu, C.-H., Lee, S.-Y., Chiang, J. C., and Tsai, P.-C.: Role of precession on the transition seasons of the Asian monsoon, *npj Climate and Atmospheric Science*, 6, 95, 2023a.
- 615 Wu, Y., Warken, S., Frank, N., Mielke, A., Chen, C.-J., Li, J.-Y., and Li, T.-Y.: Northern Hemisphere summer insolation and ice volume driven variations in hydrological environment in southwest China, *Geophysical Research Letters*, 50, e2023GL105664, 2023b.
- Wurtzel, J. B., Abram, N. J., Lewis, S. C., Bajo, P., Hellstrom, J. C., Troitzsch, U., and Heslop, D.: Tropical Indo-Pacific hydroclimate response to North Atlantic forcing during the last deglaciation as recorded by a speleothem from Sumatra, Indonesia, *Earth and Planetary Science Letters*, 492, 264–278, 2018.
- 620 Yuan, S., Chiang, H.-W., Liu, G., Bijaksana, S., He, S., Jiang, X., Imran, A. M., Wicaksono, S. A., and Wang, X.: The strength, position, and width changes of the intertropical convergence zone since the Last Glacial Maximum, *Proceedings of the National Academy of Sciences*, 120, e2217064120, 2023.
- Zhao, Y., Braconnot, P., Marti, O., Harrison, S., Hewitt, C., Kitoh, A., Liu, Z., Mikolajewicz, U., Otto-Bliesner, B., and Weber, S.: A multi-model analysis of the role of the ocean on the African and Indian monsoon during the mid-Holocene, *Climate Dynamics*, 25, 777–800,
625 2005.
- Zhou, X., Zhan, T., Tu, L., Smol, J. P., Jiang, S., Liu, X., Xu, C., and Guo, Z.: Monthly insolation linked to the time-transgressive nature of the Holocene East Asian monsoon precipitation maximum, *Geology*, 50, 331–335, 2022.